


# Spread-spectrum magnetic resonance imaging

Klaus Scheffler<sup>1,2</sup>  | Alexander Loktyushin<sup>1,3</sup> | Jonas Bause<sup>1,2</sup> | Ali Aghaeifar<sup>1,2</sup>  |  
Theodor Steffen<sup>1</sup> | Bernhard Schölkopf<sup>3</sup>

<sup>1</sup>High-Field MR Center, Max Planck Institute for Biological Cybernetics, Tübingen, Germany

<sup>2</sup>Department for Biomedical Magnetic Resonance, University of Tübingen, Tübingen, Germany

<sup>3</sup>Department of Empirical Inference, Max Planck Institute for Intelligence Systems, Tübingen, Germany

## Correspondence

Klaus Scheffler, MPI for Biological Cybernetics, Spemannstrasse 41, 72076 Tübingen, Germany.  
Email: klaus.scheffler@tuebingen.mpg.de

## Funding information

Max-Planck-Gesellschaft; Deutsche Forschungsgemeinschaft, Grant/Award Number: DFG SCHE 658/12; Max Planck Society

**Purpose:** A novel method for the acceleration of MRI acquisition is proposed that relies on the local modulation of magnetic fields. These local modulations provide additional spatial information for image reconstruction that is used to accelerate image acquisition.

**Methods:** In experiments and simulations, eight local coils connected to current amplifiers were used for rapid local magnetic field variation. Acquired and simulated data were reconstructed to quantify reconstruction errors as a function of the acceleration factor and applied modulation frequency and strength.

**Results:** Experimental results demonstrate a possible acceleration factor of 2 to 4. Simulations demonstrate the challenges and limits of this method in terms of required magnetic field modulation strengths and frequencies. A normalized mean squared error of below 10% can be achieved for acceleration factors of up to 8 using modulation field strengths comparable to the readout gradient strength at modulation frequencies in the range of 5 to 20 kHz.

**Conclusion:** Spread-spectrum MRI represents a new approach to accelerate image acquisition, and it can be independently combined with traditional parallel imaging techniques based on local receive coil sensitivities.

## KEYWORDS

acquisition acceleration, local magnetic fields, nonlinear field modulation, parallel imaging

## 1 | INTRODUCTION

Acceleration of imaging speed has been one of the most important challenges in MRI and spectroscopy during the last three decades. In the early days of MRI several minutes were required to capture a single slice of the human body using a spin echo sequence. Today, a 3D high-resolution dataset of the entire human brain can be measured within seconds. The FLASH sequence is one of the most prominent examples for rapid imaging.<sup>1</sup> With echo planar imaging a further significant acceleration was achieved by scanning multiple phase-encoded

echoes per repetition time instead of just one.<sup>2</sup> About two decades ago, the landscape for rapid MRI changed dramatically with the invention of parallel imaging techniques such as SMASH, SENSE, and GRAPPA.<sup>3-5</sup> Parallel imaging uses the spatially confined sensitivities of local radio frequency receiver coils as additional information for spatial encoding to accelerate image acquisition. The most radical and ultimate extension of parallel imaging is to use one coil per voxel (OVOC) as introduced by Hennig,<sup>6</sup> which, in principle, allows everything to be captured within microseconds. Many other rapid imaging techniques have since been proposed. For

example, UNFOLD, k-tBLAST/SENSE, or compressed sensing and its derivatives use sparse sampling in k-space and time, combined with prior knowledge to boost imaging speed further in certain applications.<sup>7-10</sup> More recently, the use of nonlinear gradients for spatial encoding such as PatLoc, FRONSAC, and O-space imaging has been proposed with the potential to provide tailored spatially varying resolution, curved imaging slices that mirror physiological geometry, and faster parallel imaging capabilities with multichannel coils.<sup>11-14</sup> Both linear and nonlinear magnetic fields can be combined and used for image encoding, which offers significantly more degrees of freedom to encode the MR signal.

In conventional imaging, the scan of k-space (which is the Fourier transformed image space) is achieved by applying linear gradients along the principal axes. In most applications, k-space is acquired line by line on a Cartesian grid, or in some implementations along projections or spirals, to name just a few. The application of additional rapid magnetic field modulations during scan of k-space has already been demonstrated in the wave-CAIPI (preceded by similar techniques such as bunched phase encoding<sup>15</sup> and zigzag sampling)<sup>16</sup> and the FRONSAC approach.<sup>12,17</sup> In wave-CAIPI, which is an extension of bunched phase encoding in combination with CAIPI,<sup>18</sup> additional phase-shifted sinusoidal modulations are applied to phase encoding gradients during the readout. This converts the original k-space scan along a straight line into an extended corkscrew trajectory. The resulting improved distribution of k-space sampling points can be used to accelerate image acquisition if combined with parallel imaging. A similar principle is used in FRONSAC, except that the additional field modulation is achieved with global second-order nonlinear shim gradients superimposed on the underlying k-space trajectory produced by linear gradients. The simulated results achieved with FRONSAC demonstrate a faster coverage of k-space (along a similar corkscrew or oscillating trajectory to that in wave-CAIPI) and thus increased imaging speed.

Here we present a novel concept to boost MR imaging speed further called spread-spectrum MRI. Spread-spectrum MRI is based on the rapid dynamic modulation of local magnetic fields produced by an array of local current loop fields instead of using global field modulations via gradient or shim coils as done in wave-CAIPI or FRONSAC. The magnetic fields produced by local current coils are modulated dynamically during signal acquisition to superimpose local and unique phase variations onto the spin distribution, which can be interpreted as a unique fingerprint onto confined regions within the object. Spread-spectrum MRI distributes or spreads the basic bandwidth of gradient-encoded magnetization frequencies using distinct modulation frequencies (or even orthogonal noise patterns) originating from a certain spatial location of the object. This spatially unique information is then utilized to disentangle different parts of the object, and thus to boost imaging speed dramatically.

In other words, spread-spectrum MRI combines local nonlinear encoding with rapid modulation of k-space trajectories.

## 2 | METHODS

### 2.1 | Experimental setup

The experimental setup used to demonstrate accelerated acquisition is illustrated in Figure 1. All measurements were performed on a 9.4 T whole-body MR scanner with a patch antenna tuned to 400 MHz.<sup>19</sup> The transmit/receive antenna was placed approximately 180 mm from the center of a cylindrical oil phantom (diameter 135 mm, length 220 mm). The phantom was surrounded by the eight local  $B_0$  coils as depicted in Figure 1. Although the patch antenna had two receive channels, the data of only a single receive channel was used for image reconstruction for simplicity. In addition to the gradients GR, GP, and GS and the radio frequency excitation, the MR scanner triggered eight parallel current amplifiers via dedicated controllers (National Instruments I/O card type PXIe-6738), which were interfaced with a LabVIEW program. The current amplifiers were connected separately to the local square-shaped  $B_0$  coils (50 mm  $\times$  50 mm, 50 windings) that injected spatially confined magnetic field modulation patterns into the measured sample placed in a cylinder with a diameter of 140 mm. Simultaneously to the acquisition of a conventional gradient echo sequence, different patterns of modulations are played out to eight local coils by the synchronized current waveform controller and amplifier. A priori measured magnetic field maps for the quantification of the  $B_0$  field change evoked by the individual local coils at a certain current are then used for reconstruction of the MR signal acquired during local modulations of  $B_0$ .

The field maps required for the spread-spectrum MRI reconstruction were determined for each coil, by performing two consecutive single-echo gradient echo measurements with a single axially oriented slice positioned approximately under the wires of the coils. The sequence triggered a half-sine-shaped current pulse with an amplitude of 0.1 A applied after the radio frequency pulse and before echo acquisition. The half-sine-length was 400  $\mu$ s and 500  $\mu$ s for the first and the second measurement, respectively. The other imaging parameters were as follows: echo time 4.8 ms, repetition time 500 ms, nominal flip angle 50°, field of view 160 mm  $\times$  160 mm, matrix size 128  $\times$  128, slice thickness 2 mm, bandwidth per pixel 410 Hz. Images were reconstructed offline using in-house-developed Matlab routines followed by the subtraction of the phase of the two images acquired with the 500  $\mu$ s and 400  $\mu$ s dephasing period. The subtraction removed any phase perturbations caused by background field inhomogeneities and permitted sufficient mapping even in proximity to the local  $B_0$  coils where the field gradient was high. The resulting difference phase maps were then converted into  $B_0$  maps for each of the eight coils.

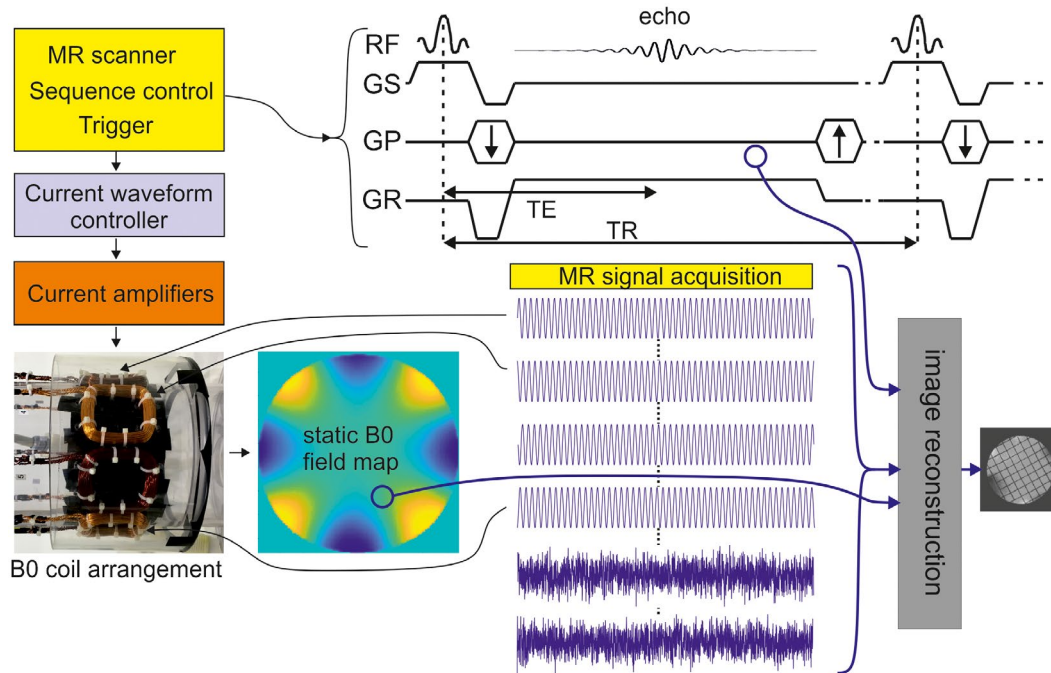


**FIGURE 1** Experimental setup of spread-spectrum imaging. The MR scanner (top left) controls the timing and execution of the gradient echo sequence (top right) and sends a trigger before each MR signal acquisition period to the current waveform controller. Eight independent current waveforms are generated, amplified by current amplifiers and applied to the eight local coils during the MR acquisition period, i.e. during the flat top of the readout gradient. For example, current modulations can be phase-shifted sine waves (as in the measurements performed in this study) or even noise patterns. The modulated and phase-encoded gradient echoes together with the knowledge of the magnetic field induced by the local coils and its corresponding current time courses are used for image reconstruction. As in conventional parallel imaging, acceleration of acquisition time is achieved by measuring only every  $n$ th phase-encoded echo

The capabilities of spread-spectrum MRI were investigated by performing a 5 kHz/3A zero-to-peak sine wave modulation on each  $B_0$  coil during signal readout. A phase increment of  $45^\circ$  between adjacent channels of the arrangement was applied. Applied current patterns were identical for each phase-encoded echo. The images with sinusoidal current modulations during the readout were acquired using the same sequence settings and slice position as the reference  $B_0$  maps, but the trigger was adjusted such that the  $B_0$  field modulations started synchronously with the data-sampling period. In order to be able to sample the full frequency spreading of the MRI signal, k-space oversampling in readout direction was increased from a factor of 2 to 8. Increasing the oversampling only changes the analog-to-digital converter dwell time but not the overall readout duration, if the bandwidth per pixel is kept at the same value. The used readout duration of 2.46 ms and gradient strength of 7.65 mT/m were therefore the same as for standard Cartesian encoding and resulted in approximately 12 field modulation cycles during each readout.

## 2.2 | Simulation setup

With the experimental setup depicted in Figure 1, which was designed to demonstrate the feasibility of accelerated imaging using spread-spectrum MRI, practical applications,

such as human brain imaging, are not feasible due to its small diameter of only 140 mm. We thus simulated an arrangement of eight square-shaped coils with an edge length of 90 mm placed on a cylinder with 250-mm diameter that provides sufficient space to fit a human head; see Figure 2. The black rectangle in Figure 2A represents the outline of the cylinder with 250 mm in diameter, where eight coils (in pink) are mounted, each rotated by  $45^\circ$  around the center of the cylinder. The color map shows the magnetic field produced by those coils in a center plane along the cylinder axis. Figure 2B is a plane perpendicular to Figure 2A along the white dashed line shown in Figure 2A. For a better visualization, a static current with opposite polarization between adjacent coils was used to calculate the field maps shown in Figure 2A and B. Figure 2C describes the magnetic field along the white line ( $\pm 90$  mm) depicted in Figure 2B. Here, a current of  $\pm 1$  A (reversed polarity for opposing coils) through a single coil winding was assumed. According to Biot-Savart's law this field decays with  $1/r$ , where  $r$  is the distance to the coil wire. A linear approximation (dotted lines in Figure 2C) results in a gradient strength of about  $20 \mu\text{T/m}$  (averaged along 180 mm) and  $10 \mu\text{T/m}$  (averaged over 100 mm). For the simulations based on this setup, a reference image (depicted schematically in Figure 2B) acquired with a conventional gradient echo

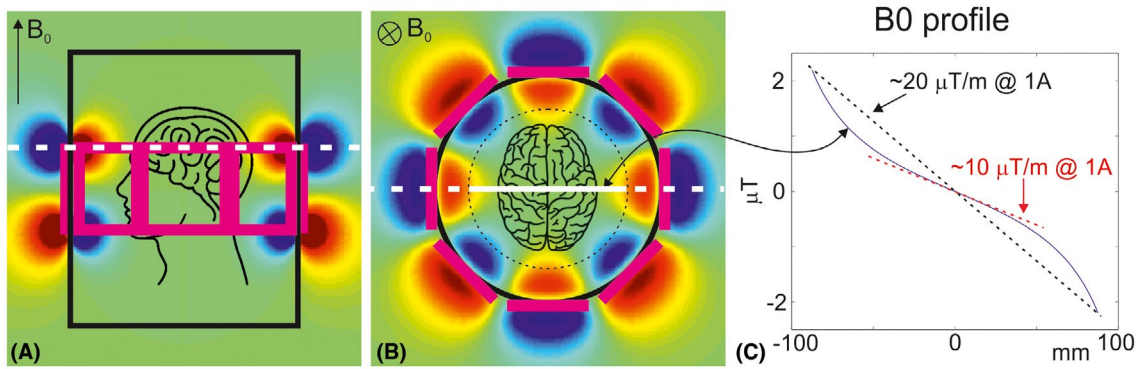


**FIGURE 2** Illustration of the setup used for simulations. The underlying color maps in A and B represent magnetic fields generated by the eight local coils at a plane through the center of the cylinder (A) and a plane along the dashed white line in A (B). These maps were calculated using Biot-Savart's law and assuming opposite currents between adjacent coils. The resulting magnetic field within the dotted circle (180-mm diameter) and along the white line in B is shown in C including two linear field approximations (dotted lines) of 10 and 20  $\mu\text{T/m}$  for a current of 1 A (and  $-1$  A for the opposing coil) through a coil with a single turn

sequence at 9.4T with an in-plane resolution of  $0.85 \text{ mm} \times 0.85 \text{ mm}$  and a matrix size of  $256 \times 256$  was used. Applied reconstruction algorithms are described in the following.

### 2.3 | Image reconstruction

In the presence of locally modulated magnetic fields, the measured signal  $\mathbf{s}$  at a k-space coordinate  $\mathbf{k}$  at time point  $t$  is given by the following equation:

$$\mathbf{s}(\mathbf{k}, t) = \iiint \mathbf{m}(\mathbf{r}) \mathbf{p}(\mathbf{r}) \exp\left(-i\gamma(\mathbf{k}(t) \mathbf{r} + \sum_c \mathbf{B}_c(\mathbf{r}) \int_{t_1}^t f_c(\tau) d\tau)\right) dx dy dz \quad (1a)$$

$$\mathbf{k}(t) = \int_0^t \mathbf{g}(\tau) d\tau \quad (1b)$$

We assume that the measurement is performed with a single excitation/acquisition coil with a complex-valued sensitivity profile denoted as  $\mathbf{p}(\mathbf{r})$ . Without loss of generality, the terms describing relaxation effects are omitted in spatial encoding model (Equation (1a) and (1b)). The phase of the exponential term is composed of two parts. The term  $\mathbf{k}(t)$  describes the k-space position related to the spatially linear gradients that are used to perform frequency and phase

played separately to each coil element  $c$ . The  $B_0$  field profile of each coil element  $c$  is indicated by  $\mathbf{B}_c(\mathbf{r})$ , which was measured with the previously described two gradient echo measurements.  $\mathbf{m}(\mathbf{r})$  is the object image to be reconstructed, and  $t_1$  denotes the time of beginning of the modulation.

The continuous model has a discrete counterpart, where spatial encoding terms are described by the elements of the encoding matrix  $\mathbf{E}$ . Without loss of generality, let us consider a case in which a single 2D slice is acquired. Let  $K_x$  and  $K_y$  be the number of acquired k-space points in read-out and phase-encode direction, respectively. Further, let  $N_x$  and  $N_y$  be the number of pixels in spatial domain. We acquire a complex-valued spectrum  $\mathbf{s} \in \mathbb{C}^{K_x \times K_y}$ , and want to reconstruct the image  $\mathbf{m} \in \mathbb{C}^{N_x \times N_y}$ . The image acquisition process with local magnetic field modulation can be described by a discrete linear operator  $\mathbf{E} \in \mathbb{C}^{(K_x K_y) \times (N_x N_y)}$ . The acquisition process can therefore be described by a linear equation  $\mathbf{s} = \mathbf{E} \mathbf{m}$ . In case the currents injected into the loops are zero, the encoding matrix is an orthonormal Fourier transform matrix  $\mathbf{E} = \mathbf{F}$ . For ease of indexing let's reshape the encoding matrix as  $\mathbf{E} \in \mathbb{C}^{K_x \times K_y \times N_x \times N_y}$ . In the experiments and simulations described earlier a sine wave modulation  $f_c(t) = \sin(t)$  of the local fields was applied that was identical for each phase encoding line. The elements of the matrix  $\mathbf{E}$  are then given by:

$$\mathbf{E}_{i,j,l,m} = \mathbf{F}_{i,j,l,m} \exp\left(-i\gamma \frac{\sum_c (a_c \mathbf{B}_{c,l,m} (\cos(2\pi w t_1 + \theta_c) - \cos(2\pi w t_i + \theta_c)))}{w}\right) \quad (2)$$

encoding ( $\mathbf{g}$ : linear magnetic field gradient vector,  $\mathbf{r}$ : spatial vector,  $\tau$  and  $t$ : time). The second term  $\sum_c \mathbf{B}_c(\mathbf{r}) \int_{t_1}^t f_c(\tau) d\tau$  corresponds to the sum of fields induced by the local magnetic field coils subject to an arbitrary waveform  $f_c$ . The waveform  $f_c$  represents the (unitless) current time course

Here,  $\mathbf{B}_c \in \mathbb{C}^{C \times N_x \times N_y}$  is the  $B_0$  field profile of a coil element  $c$  (where  $C$  is the total number of coil elements),  $w$  is the frequency of the spread-spectrum modulation,  $a_c$  is the modulation current amplitude,  $\theta_c$  is the phase offset of the modulation. An extension of the model to the case of accelerated



acquisition is straightforward, for example, reduction of the number of phase encodings  $j \in K_y$  and involves decreasing the number of rows in the matrix  $\mathbf{E}$ .

The image can be reconstructed by solving a linear equation systems  $\mathbf{s} = \mathbf{E}\mathbf{m}$ , which can be done for both general (Equation (2)) and separable (Equation (4); see following discussion) cases. In MR signal acquisitions with geometry factors ( $g$ -factor (4)) close to unity, computing the pseudoinverse of the encoding matrix  $\mathbf{E}$  and applying it to the measured  $k$ -space allow for a simple one-shot reconstruction. Otherwise, in case the  $g$ -factor is greater than unity, inversion of the system can be unstable and results become noisy. In such case, the following regularized optimization problem is solved:

$$\hat{\mathbf{m}} = \arg \min_{\mathbf{m}} (\|\mathbf{s} - \mathbf{E}\mathbf{m}\|_2^2 + \lambda |\text{TV}(\mathbf{m})|) \quad (3)$$

The regularization coefficient  $\lambda$  sets the weight of the total variation term ( $\text{TV}(\mathbf{m})$ ) that penalizes blurring and ghosting artifacts in the reconstruction. The regularization term can be seen

$$s[k_x, y] = \sum_x \mathbf{m}[x, y] \exp \left( -i2\pi (k_x x / K_x) + \sum_c \mathbf{B}_c[x, y] \frac{\cos(2\pi w t_1 + \theta_c) - \cos(2\pi w t_{k_x} + \theta_c)}{w} \right) \quad (4)$$

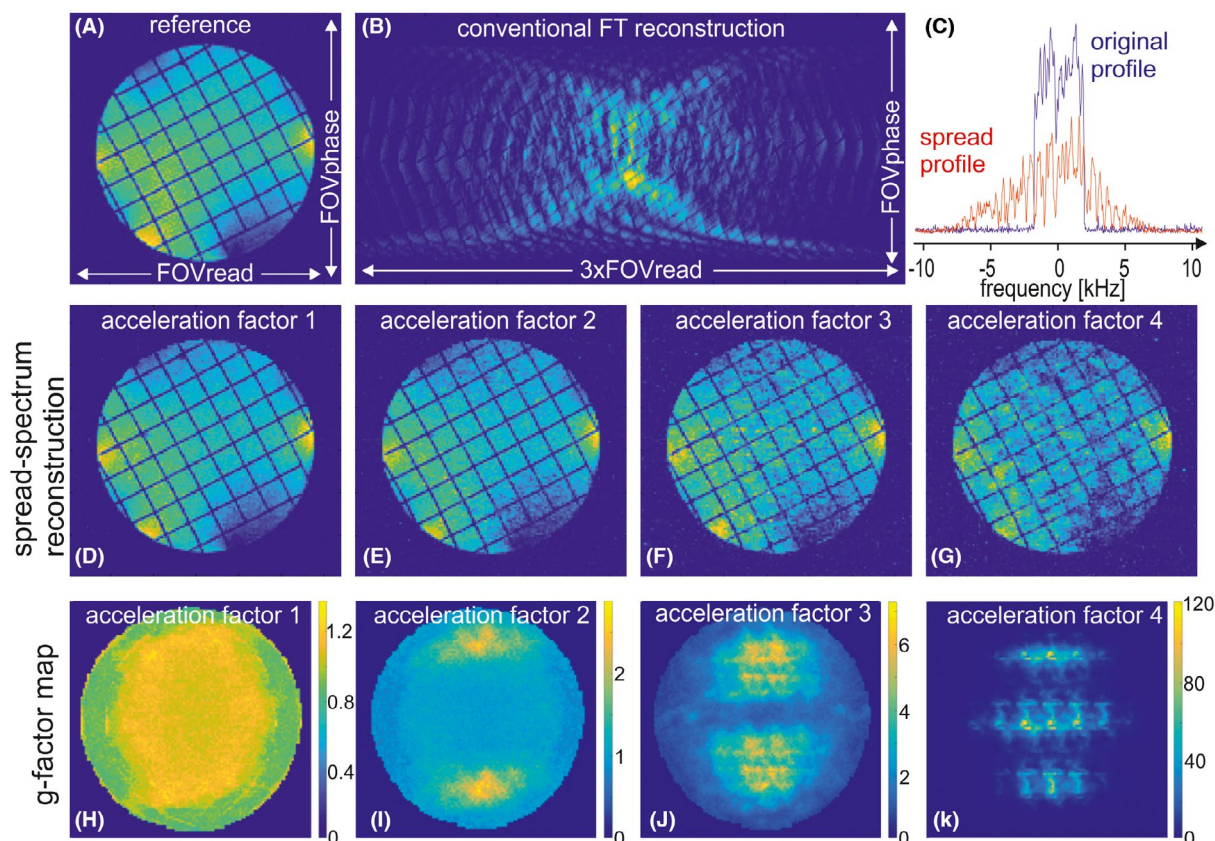


**FIGURE 3** Experimental results achieved with spread-spectrum MRI. Top row: The application of phase-shifted 5-kHz current modulations leads to a spreading of the reference image A along readout direction (left–right) in the conventionally reconstructed image B. This frequency spread is also visible in the profiles (magnitude of the Fourier transformed central  $k$ -space line along readout direction with and without modulation) shown in C. The middle row shows spread spectrum reconstructed images of measured data with increasing acceleration factors, and the bottom row the corresponding  $g$ -factor maps, which indicate the noise amplification

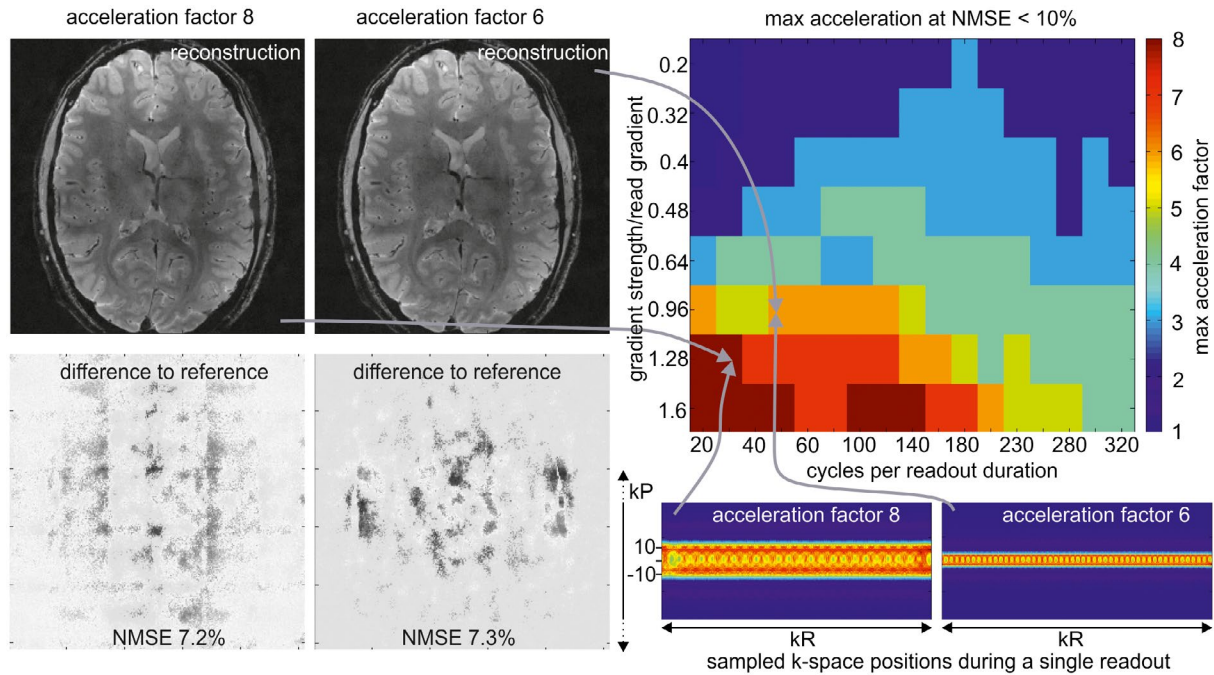


**FIGURE 4** Simulated results achieved with spread-spectrum MRI. The column on the left shows simulated examples of reconstructed brain images accelerated by a factor of 6 and 8 and corresponding differences to the reference image. A modulation frequency of 24 and 32 cycles per readout gradient duration and a (linearly approximated) gradient strength of 1.28 and 0.96 relative to the readout gradient strength were applied to the local coils in the case of eight-fold and six-fold acceleration, respectively. These two combinations of modulation frequency and strength are marked by arrows in the matrix plot shown right. This plot gives an overview of achievable acceleration factors confined to reconstruction errors of below 10% NMSE, as a function of applied modulation strength and frequency to the local coils. Units are scaled to the strength and duration of the applied readout gradient. The two figures on the bottom right depict the sampled points in k-space along read (kR) and phase (kP) direction for acceleration factors of 6 and 8. Spreading along kP is about  $\pm 10$  and  $\pm 4$  phase encoding steps. NMSE, normalized mean square error

Here,  $k_x$  is the k-space index of the data sample in readout direction. In this representation, it is easy to see that the complex coefficients at each line in the hybrid space  $\mathbf{s}_y$  only depend on the magnetization values  $\mathbf{m}_y$  from the same line. In other words, no mixing of image voxel values in phase encode direction occurs and the image content is spread purely in readout direction. An advantage of such formulation is that the image reconstruction process can be made separable in phase encode direction in spatial domain, which results in smaller linear systems to be solved and faster convergence. However, in the more general case of arbitrary modulations for each phase encoding step or for non-Cartesian trajectories the optimization scheme shown in Equation 3 needs to be solved.

### 3 | RESULTS

#### 3.1 | Experimental results

Experimental results achieved with this setup are summarized in Figure 3. Conventional 2D Fourier reconstruction of the phase-encoded and sine-wave-modulated echoes is shown in Figure 3B demonstrating a spread of the reference image along the readout direction. The profiles shown in Figure 3C are the magnitude of the Fourier transformed gradient echo acquired at the center of k-space

(no phase encoding) without (original profile, blue) and with 5-kHz field modulation (spread profile, red), showing a frequency-spread profile of about  $\pm 5$  kHz of the original profile. A phase increment of the 5-kHz sine waves of  $45^\circ$  between adjacent coils was applied. The second row shows reconstructed images acquired with local current modulation and acceleration factors of 1 to 4, i.e. using each k-space line (D), every other (E), every third (F), and every fourth k-space line (G), respectively. The degradation of image quality with increasing acceleration is quantified in Figure 3H to K as g-factor maps based on the pseudoreplica method.<sup>21</sup> G-factors in the range of 1 to 1.5 represent only a minor amplification of reconstruction-related noise in the accelerated images, which is the case for the reference image H and the two-fold accelerated image I. Image degradation for higher g-factors is visible in Figure 3F and G. Reconstruction time was about 5 seconds on an Intel Core i7-3770K CPU operating at 3.50 GHz in combination with a Nvidia GeForce GTX TITAN GPU.

#### 3.2 | Simulated results

The experimental results shown in Figure 3 have been acquired with a modulation frequency of 5 kHz at 3A

(zero-to-peak), which was the performance limit of the connected analog current amplifiers. Numerical simulations of this setup (not shown here) were able to demonstrate a theoretical acceleration factor up to 10 (with an image degradation of less than 10% normalized mean square error [NMSE] compared to the reference image) for modulation frequencies in the range of 10 to 20 kHz at peak currents of 6 to 8 A.

Examples of simulated reconstructions of the reference brain slice with acceleration factors of 6 and 8 using different modulation strength and frequency are depicted in Figure 4. As the reconstruction error is below 10% NMSE no differences in reconstruction quality or differences to the reference image (not shown here) are visible. The color map matrix shown at the right top represents maximum achievable acceleration factors resulting in reconstruction errors of below 10% NMSE as a function of applied modulation field strength and frequency to the local coils. To allow generalization of these simulations, the strength of the modulation fields is given as the ratio of the approximated linear field gradient strength generated by the local coils and the applied readout field gradient strength. The modulation frequency is given as the number of sine wave cycles per duration of the readout gradient.

In conventional imaging based on linear gradient field encoding, single points in k-space are sampled along a Cartesian trajectory or grid. Using nonlinear magnetic fields for encoding spreads each single point in k-space to a pattern or stamp of certain shape and size, similar to the O-space or FRONSAC methods that are based on spatially quadratically varying magnetic fields.<sup>12-14</sup> The k-space pattern sampled along a single readout is shown in Figure 4 right bottom for two combinations of modulation strengths and frequencies. Without additional modulation, the sampling pattern is a single straight line along readout direction  $k_R$ . The spread of those patterns along phase encode direction (about  $\pm 10$  and  $\pm 4$  phase encoding steps for accelerations of 8 and 6, respectively) enables reduction of the number of linear phase encoding steps, leading to possible accelerations of a factor of 6 and 8. In general, higher-modulation amplitudes or fields increase k-space coverage along phase direction ( $k_P$ ) and thus allow for higher acceleration. This is presented on the color map showing increasing maximum possible acceleration factors as a function of modulation strength.

## 4 | DISCUSSION

Spread-spectrum MRI is based on rapid local magnetic field modulation that enables acceleration of image acquisition. Acceleration factors of up to 4 were demonstrated experimentally in a phantom study using eight local coils modulated with 5 kHz. In order to estimate the practical performance

and limits of spread-spectrum MRI for human brain imaging, a larger setup consisting of eight coils arranged on a cylinder with 250 mm was simulated. In this simulation, only a single slice positioned in the region of largest field variations was considered, and local field modulations were combined with a conventional Cartesian k-space sampling using a linear readout gradient GR preceded by a stepwise increased phase encoding gradient GP. The required field strength generated by the local coils to achieve a certain acceleration factor scales (linearly, if local fields are approximated by a linear gradient as depicted in Figure 2C) with the strength of the used readout gradient GR. Depending on the targeted acceleration factor, the required local field strength is in the order of 20% to 150% of the strength of the applied readout gradient GR. Assuming a readout gradient strength GR of 10 mT/m (GR is in the order of 5 mT/m for conventional imaging, and 20 to 30 mT/m for fast imaging such as EPI and balanced SSFP) this corresponds to a required local field of 2 to 15 mT/m. In the approximation of a linear local field modulation, a pair of opposing wires with opposite current direction produce a gradient field of about 10  $\mu\text{T/m}$  per ampere, as shown in Figure 2C, Methods section. As an example, a coil with 25 turns will then generate a gradient field of 0.25 mT/m, and currents of 8 to 60 A are required to achieve a local modulation field of 2 to 15 mT/m. The inductance of such a 90 mm  $\times$  90 mm, 25-turn coil is on the order of 100  $\mu\text{H}$  (measured experimentally), resulting in a required driving voltage of 5 V (at 8 A and 1 kHz) up to 375 V (at 60 A and 10 kHz). This rough estimation of required currents and voltages is in the range of what small to medium current amplifiers are able to deliver. However, these estimations scale (about linearly) with the gradient strength used to sample k-space, and they scale (nonlinearly as depicted in the color map in Figure 4) with the targeted acceleration factor. For example, for an acceleration factor of 3 and a moderate readout gradient strength of 5 mT/m, currents in the range of 2 A to 3 A and frequencies of 4 kHz to 5 kHz are required, which leads to driving voltages of only about 5 V to 10 V for a 25-turn coil. Therefore, the required experimental effort for accelerated spread-spectrum MRI strongly depends on the specific application.

The presented experimental and theoretical results are based on phase-shifted sinusoidal modulation patterns. Thus, the resulting magnetic field pattern rotates within the imaging plane (Figure 2B) with the frequency of the applied sine wave. This corresponds to a rotation of the  $1/r$  decaying magnetic fields shown in Figure 2C within the imaging slice. Using a linear field approximation (dashed lines in Figure 2C) the local coils generate a linear magnetic field gradient that rotates in a plane perpendicular to  $B_0$ . In this linear approximation, the sampling of the measured MR signal in k-space is a superposition of a circle trajectory (from the modulated local coils) with a linear trajectory (from the readout gradient). This sampling trajectory is similar to the



wave-CAIPI corkscrew trajectory,<sup>17</sup> which is generated by sinusoidal modulation of the linear gradients. The use of local, nonlinear magnetic modulation fields spreads this corkscrew trajectory into a dense band of k-space sampling points, as depicted in Figure 4. These trajectories show a certain similarity to the trajectories generated by the O-space or FRONSAC method<sup>12-14</sup> resulting in a space variant resolution. However, in spread-spectrum MRI each single coil can be driven independently, leading to a much higher flexibility and degrees of freedom in possible modulation patterns as compared to only quadratically varying fields used in O-space or FRONSAC. This also offers the unique possibility to adapt local modulation fields to the underlying k-space trajectory generated by the linear imaging gradients with the goal to optimize the sampled k-space density across k-space. Independent local field modulation also allows optimization of combined acceleration with parallel imaging.

The achievable acceleration factor with spread-spectrum MRI depends on the field strength that is produced by the local modulation coils, and it varies along the spatial position along the local coil arrangement. As depicted in Figure 2, the strongest field modulation is along the dotted white line positioned along the coil windings perpendicular to the main static magnetic field  $B_0$  in z-direction. Thus, possible acceleration factors significantly depend on the position and orientation of the imaging slice, and even no acceleration is possible for slices centered between opposing coil windings, i.e. where local fields from the coils cancel each other. Therefore, imaging acceleration is closely linked to the arrangement and number of local coils as well as to the spatial position and orientation of the imaging slice or position of the imaging volume for 3D imaging. This, however, also offers the possibility to design dedicated coil arrangements adapted to the specific requirements of certain imaging applications. As for any sequence, SNR is proportional to the square root of the total acquisition time (or sum of acquired ADC intervals) plus potential penalties for ill-conditioned problems reflected in an increased g-factor or NMSE. Therefore, presented acceleration factors of 6 or 8 shown in Figure 4 have a reduced SNR of  $\sqrt{6}$  or  $\sqrt{8}$ , respectively.

Rapidly changed magnetic fields may stimulate nerves or muscles by inducing electric fields. The threshold for peripheral nerve stimulation is on the order of 50 T/s (rheobase, infinite duration of magnetic field change dB/dt).<sup>22</sup> Assuming a local magnetic field modulation of 20 mT/m at 10 kHz to achieve high acceleration factors corresponds to a magnetic field change of about 40 T/s at a distance of 10 cm from the center of the specific coil arrangement shown in Figure 2A. Application of these rapidly changing fields thus seems to be feasible for human brain studies and is assumed to be even less problematic if smaller diameters of the  $B_0$  arrangement can be used as in case of limb imaging.

This study was restricted to 2D imaging in combination with an underlying Cartesian k-space sampling, and the use

of only one receiver coil. Furthermore, all modulation coils were mounted at identical z-position on the cylinder. A further direction is thus to explore the potential of an array of local modulation coils distributed along the z and angular direction, similar to what is used for local shimming using matrix coils.<sup>23</sup> This will increase the flexibility of modulation patterns along all principal axes, which is mandatory for accelerated 3D imaging. Similarly, other k-space trajectories such as spirals or radial sampling combined with temporally varying local modulation patterns might further increase acquisition speed (see also O-SPACE reference). Furthermore, spread-spectrum MRI can be combined with parallel imaging, which is particularly advantageous if the overlap of individual radio frequency receive coil sensitivities and current coil field profiles is minimized. In case of spatially separated radio frequency coil and current coil profiles, individual acceleration factors generated with both spread-spectrum MRI and parallel imaging might be used independently for acquisition acceleration, resulting in a multiplication of acceleration factors.

## ACKNOWLEDGMENTS

This work was supported by the Max Planck Society and the German research foundation (Reinhart Koselleck Project, DFG SCHE 658/12).

## AUTHOR CONTRIBUTIONS

Klaus Scheffler, Alexander Loktyushin, and Jonas Bause contributed equally to this work.

## ORCID

Klaus Scheffler  <https://orcid.org/0000-0001-6316-8773>

Ali Aghaeifar  <https://orcid.org/0000-0002-6964-0992>

## REFERENCES

- Haase A, Frahm J, Matthaei D, Hänicke W, Merboldt KD. FLASH imaging: rapid NMR imaging using low flip-angle pulses. 1986. *J Magn Reson*. 2011;213:533–41.
- Mansfield P. Multi-planar image formation using NMR spin echoes. *J Phys C: Solid State Phys*. 1977;10:L55–L58.
- Sodickson DK, Manning WM. Simultaneous acquisition of spatial harmonics (SMASH): fast imaging with radiofrequency coil arrays. *Magn Reson Med*. 1997;38:591–603.
- Pruessmann KP, Weiger M, Scheidegger MB, Boesiger P. SENSE: sensitivity encoding for fast MRI. *Magn Reson Med*. 1999;42:952–962.
- Griswold MA, Jakob PM, Heidemann RM, et al. Generalized auto-calibrating partially parallel acquisitions (GRAPPA). *Magn Reson Med*. 2002;47:1202–1210.
- Hennig J, Zhong K, Speck O. MR-Encephalography: fast multi-channel monitoring of brain physiology with magnetic resonance. *Neuroimage*. 2007 Jan 1;34:212–9.



7. Madore B, Glover GH, Pelc NJ. Unaliasing by fourier-encoding the overlaps using the temporal dimension (UNFOLD), applied to cardiac imaging and fMRI. *Magn Reson Med.* 1999;42:813–828.
8. Parrish T, Hu X. Continuous update with random encoding (CURE): a new strategy for dynamic imaging. *Magn Reson Med.* 1995;33:326–336.
9. Tsao J, Boesiger P, Pruessmann KP. k-tBLAST and k-t SENSE: dynamic MRI with high frame rate exploiting spatiotemporal correlations. *Magn Reson Med.* 2003;50:1031–1042.
10. Lustig M, Donoho DL, Pauly JM. Sparse MRI: the application of compressed sensing for rapid MR imaging. *Magn Reson Med.* 2007;58:1182–1195.
11. Hennig J, Welz AM, Schultz G, et al. Parallel imaging in non-bijective, curvilinear magnetic field gradients: a concept study. *Magma.* 2008;21:5–14.
12. Wang H, Tam LK, Constable RT, Galiana G. Fast rotary nonlinear spatial acquisition (FRONSAC) imaging. *Magn Reson Med.* 2016;75:1154–1165.
13. Stockmann JP, Ciris PA, Galiana G, Tam LK, Constable RT. O-space images: highly efficient parallel imaging using second-order nonlinear fields as encoding gradients with no phase encoding. *Magn Reson Med.* 2010;64:447–56.
14. Wang H, Tam L, Kopanoglua E, Peters DC, Constable RT, Galiana G. O-space with high resolution readouts outperforms radial imaging. *Magn Reson Imaging.* 2017;37:107–115.
15. Moriguchi H, Duerk JL. Bunched phase encoding (BPE): a new fast data acquisition method in MRI. *Magn Reson Med.* 2006;55:633–648.
16. Breuer FA, Moriguchi H, Seiberlich N, et al. Zigzag sampling for improved parallel imaging. *Magn Reson Med.* 2008;60:474–478.
17. Bilgic B, Gagoski BA, Cauley SF, et al. Wave-CAIPI for highly accelerated 3D imaging. *Magn Reson Med.* 2006;73:2152–2162.
18. Breuer F, Blaimer M, Heidemann RM, Mueller MF, Griswold MA, Jakob PM. Controlled aliasing in parallel imaging results in higher acceleration (CAIPIRINHA) for multi-slice imaging. *Magn Reson Med.* 2005;53:684–691.
19. Hoffmann J, Shajan G, Budde J, Scheffler K, Pohmann R. Human brain imaging at 9.4 T using a tunable patch antenna for transmission. *Magn Reson Med.* 2013;69:1494–1500.
20. Ulyanov D, Vedaldi A, Lempitsky V. Deep image prior. 2017. arXiv preprint arXiv:1711.10925.
21. Robson PM, Grant AK, Madhuranthakam AJ, Lattanzi R, Sodickson DK, McKenzie CA. Comprehensive quantification of signal-to-noise ratio and g-factor for image-based and k-space-based parallel imaging reconstructions. *Magn Reson Med.* 2008;60:895–907.
22. Schaefer DJ, Bourland JD, Nyenhuis JA. Review of Patient safety in time-varying gradient fields. *J Magn Reson Imaging.* 2000;12:20–29.
23. Juchem C, Nixon TW, McIntyre S, Rothman DL, De Graaf RA. Magnetic field modeling with a set of individual localized coils. *J Magn Reson.* 2010;204:281–289.

**How to cite this article:** Scheffler K, Loktyushin A, Bause J, Aghaeifar A, Steffen T, Schölkopf B. Spread-spectrum magnetic resonance imaging. *Magn Reson Med.* 2019;82:877–885. <https://doi.org/10.1002/mrm.27766>